BIOCHEMISTRY
including biophysical chemistry & molecular biology

Article

pubs.acs.org/biochemistry

Evidence for Direct Binding between HetR from *Anabaena* sp. PCC 7120 and PatS-5

Erik A. Feldmann,[†] Shuisong Ni,[†] Indra D. Sahu,[†] Clay H. Mishler,[†] Douglas D. Risser,[‡] Jodi L. Murakami,[‡] Sasa K. Tom,[‡] Robert M. McCarrick,[†] Gary A. Lorigan,[†] Blanton S. Tolbert,[†] Sean M. Callahan,[‡] and Michael A. Kennedy*[,†]

[†]Department of Chemistry and Biochemistry, Miami University, Oxford, Ohio 45056, United States

[‡]Department of Microbiology, University of Hawaii, Honolulu, Hawaii 96822, United States

Supporting Information

ABSTRACT: HetR, master regulator of heterocyst differentiation in the filamentous cyanobacterium *Anabaena* sp. strain PCC 7120, stimulates heterocyst differentiation via transcriptional autoregulation and is negatively regulated by PatS and HetN, both of which contain the active pentapeptide RGSGR. However, the direct targets of PatS and HetN remain uncertain. Here, we report experimental evidence for direct binding between HetR and the C-terminal RGSGR pentapeptide, PatS-5. Strains with a *hetR* allele coding for conservative substitutions at residues 250−256 had altered patterns of heterocysts and, in some cases, reduced sensitivity to PatS-5. Cysteine scanning mutagenesis coupled with electron paramagnetic resonance (EPR) spectroscopy showed quenching of spin label motion at HetR amino acid 252 upon titration with PatS-5, indicating direct binding of PatS-5 to HetR. Gel shift assays indicated that PatS-5 disrupted binding of HetR to a 29 base pair inverted-repeat-containing DNA sequence upstream from *hetP*. Double electron−electron resonance EPR experiments confirmed that HetR existed as a dimer in solution and indicated that PatS-5 bound to HetR without disrupting the dimer form of HetR. Isothermal titration calorimetry experiments corroborated direct binding of PatS-5 to HetR with a K_d of 227 nM and a 1:1 stoichiometry. Taken together, these results indicated that PatS-5 disrupted HetR binding to DNA through a direct HetR/PatS interaction. PatS-5 appeared to either bind in the vicinity of HetR amino acid L252 or, alternately, to bind in a remote site that leads to constrained motion of this amino acid via an allosteric effect or change in tertiary structure.

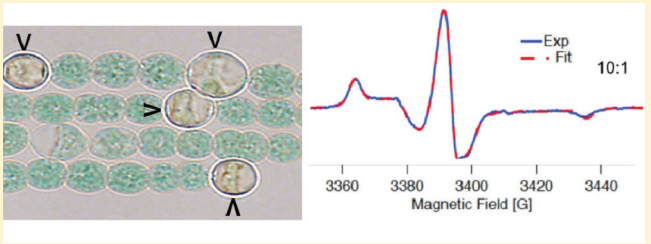

Cellular differentiation and patterning are fundamental concepts in the field of developmental biology. One of the earliest known examples of cell differentiation is that of ancient filamentous cyanobacteria, which, under pressure of nitrogen starvation, evolved the capability to fix atmospheric N_2 using specialized terminally differentiated cells called "heterocysts"[1−12] more than 2 billion years ago.[13,14] Heterocyst differentiation in filamentous cyanobacteria evolved as a means of isolating oxygenic photosynthesis associated with CO_2 fixation in vegetative cells from oxygen-sensitive nitrogenases that carry out nitrogen fixation in heterocysts.[15,16] Soluble nitrogen-containing compounds generated as a result of nitrogen fixation in heterocysts are shared with neighboring vegetative cells to sustain continued growth of the organism (see discussion by Haselkorn[17] regarding intercellular transport in filamentous cyanobacteria). Under conditions of nitrogen starvation, a pattern is established in which approximately every tenth cell along the filament is terminally differentiated into a heterocyst.[18,19] Heterocysts support nitrogenase-based N_2 fixation by generating a microoxic environment within the cell that involves production of two additional layers external to the outer membrane found in vegetative cells, including a heterocyst-specific glycolipid layer and a heterocyst envelope polysaccharide layer.[20−22] Initiation of heterocyst differentiation, pattern formation, and pattern maintenance are regulated by small signaling molecules and a host of different genes in a process that resembles signaling pathways of higher eukaryotic organisms.[10,11]

The *hetR* gene plays a central role in regulation of heterocyst differentiation.[23] The master regulatory protein, HetR, controls heterocyst differentiation through transcriptional autoregulation[24] and responds to two heterocyst differentiation inhibitors, PatS and HetN, both of which contain the active pentapeptide RGSGR.[24−26] Interestingly, *hetR* and *patS* genes are widespread throughout both nonheterocyst-forming and heterocyst-forming filamentous cyanobacteria, suggesting that their evolutionary role may have emerged before heterocyst differentiation appeared.[27] While much has been learned about regulation of heterocyst differentiation in recent years, the molecular level interactions between HetR, PatS, and HetN during regulation of heterocyst differentiation are still not well understood. There

Received: August 5, 2011
Revised: September 22, 2011
Published: September 26, 2011

is growing experimental evidence that PatS and HetN control pattern formation by establishing concentration gradients along the filament that promote degradation of HetR in an activator-inhibitor type manner;[28] however, the precise mechanism for how HetR interacts with PatS and HetN remains unknown.

HetR is a 299 residue DNA binding transcriptional regulator believed to be active as a homodimer.[29] It has been reported that HetR dimer formation involves a disulfide bridge at position C48, and that mutation of C48 to alanine abolished both dimerization and binding activity to its own DNA promoter *in vitro*.[29] It has also been reported that HetR has Ser-type autoproteolytic activity[30,31] mediated through Ser152.[32] However, Risser and Callahan have reported that Cys48 and Ser152 in HetR from *Anabaena* are not required for proper heterocyst differentiation.[33] The cause of the contradictory observations has not yet been resolved.

PatS is a short peptide, predicted to be 13 or 17 amino acids, that acts as a negative regulator of heterocyst differentiation.[25] It is thought that a shorter, processed form of PatS acts as a diffusible signal molecule.[25,34] The RGSGR carboxyl terminus of PatS (PatS-5) inhibits heterocyst differentiation when added to culture medium,[25] and has been shown *in vitro* to inhibit binding of HetR to a DNA sequence upstream from its own promoter.[29,33] It has also been shown that a R223W mutant of HetR was insensitive to *in vivo* overexpression of both PatS and HetN.[35] However, the mechanism of PatS-5 disruption of HetR binding to DNA, and the molecular level cause of loss of R223W HetR sensitivity to PatS, remains unknown.

A molecular-level understanding of the biochemical mechanism of action of PatS-5 has not been established. While it has been widely assumed that PatS-5 disrupts HetR binding to DNA through a direct interaction between PatS-5 and HetR, based on observations reported in the literature,[29,33,35] it is alternatively possible that PatS-5 disrupts the HetR−DNA complex through a direct interaction between PatS-5 and the DNA. This possibility is worth considering given that the amino acid sequence of PatS-5, RGSGR, with its symmetrically positioned arginines, is similar to that of the well-established DNA-binding "AT-hook" motif,[36] which has the minimal amino acid consensus sequence PRGRP[37] with both symmetrically positioned arginine residues conferring, and being required for, DNA binding. The AT-hook is the fundamental DNA binding motif of the HMG-I(Y) (aka HMGA) subfamily of nonhistone high mobility group chromatin proteins,[38,39] also known as "architectural transcription factors",[37,40,41] with each HMG-I(Y) protein containing three AT-hooks. When bound to DNA, the AT-hook adopts a crescent-shaped structure that binds AT-rich DNA sequences through nonspecific electrostatic interactions between the negatively charged phosphodiester DNA backbone and the positively charged arginine side chains that insert into the DNA minor groove.[42] Each PRGRP AT-hook motif spans 5 to 6 DNA base pairs.[36] Given the similarity between the amino acid sequences of the AT-hook motif and PatS-5, and the observation that a single AT-hook confers DNA binding capability,[37] it is plausible that PatS-5 might also interact with DNA via nonspecific electrostatic interactions through its symmetrically positioned pair of arginine residues. The lack of three-dimensional structures of most heterocyst regulatory proteins and any complexes involving PatS-5 has impeded progress toward achieving a complete molecular level understanding of regulation of heterocyst differentiation. However, the recent report of the crystal structure of HetR from *Fischerella*[43] should begin to open the door to a better understanding of this regulatory process at the molecular level.

Here, we report several major findings that should advance the understanding of regulation of heterocyst pattern formation in *Anabaena*, including (1) discovery of a region of HetR containing amino acids 250−256 necessary for HetR sensitivity to PatS-5; (2) evidence that PatS binds directly to HetR from a combination of cysteine scanning mutagenesis and continuous wave (CW) electron paramagnetic resonance (EPR) spectroscopy; (3) determination that PatS-5 binds directly to HetR without disrupting the HetR homodimer based on double electron−electron resonance (DEER) EPR experiments; and, finally, (4) corroboration that PatS-5 binds directly to HetR with a 1:1 stoichiometry and measurement of the dissociation constant for HetR binding to PatS-5 using isothermal titration calorimetry.

MATERIALS AND METHODS

Bacterial Strains and Growth Conditions. Growth of *Escherichia coli* and *Anabaena* sp. strain PCC 7120 and its derivatives, concentrations of antibiotics, induction of heterocyst formation, regulation of the *petE* and *nir* promoters, and photomicroscopy were as previously described.[33] Plasmids were conjugated from *E. coli* to *Anabaena* sp. strain PCC 7120 and its derivatives as previously described.[44]

Plasmid Construction for Making Chromosomal Alleles. Strains of *Anabaena* and plasmids used in this study are described in Supporting Information Table S1. Plasmids pJM100, pJM101, pJM102, pJM103, pST211, pJM104, pJM105, and pDR219 are suicide vectors used to replace the chromosomal *hetR*-locus with *hetR(R250K)*, *hetR(A251G)*, *hetR(L252V)*, *hetR(E253D)*, *hetR(E254D)*, *hetR(L255V)*, *hetR-(D256E)* and *hetR(E254G)*, respectively. Overlap extension PCR was used to generate each of the mutant *hetR* alleles except *hetR(E254D)* and *hetR(E254G)* that used the inner primers listed in Supporting Information Table S2 with names corresponding to that of the resulting substitution with the outer primers PhetR-BamHI-F and hetR 3′ Seq. The resulting PCR products were cloned into plasmid pDR327 as NcoI−SpeI fragments to create plasmids pJM100, pJM101, pJM102, pJM103, pJM104, and pJM105. Plasmids pST211 and pDR219 were generated in a similar fashion, but outer primer hetR-SacI-SpeI-R was used in place of hetR 3′ seq for pST211 and previously published inner primers[33] were used to create *hetR(E254G)* in pDR219.

Construction of Strains Containing Mutant Alleles. Strains of *Anabaena* with mutant alleles of *hetR* in place of the wild-type *hetR* were created as described previously[28] using the *hetR*-deletion strain UHM103 and plasmids pJM100, pJM101, pJM102, pJM103, pST211, pJM104, pJM105, and pDR219 to generate strains UHM163, UHM164, UHM165, UHM166, UHM167, UHM168, UHM169, and UHM122, respectively. Strains with *hetR(E253D)* and *hetR(E254D)* are single recombinants in which the entire plasmid is in the *hetR* chromosomal locus, whereas the others are the same as PCC 7120 except for the change in *hetR* sequence.

***In Vivo* PatS-5 Sensitivity Assays.** Duplicate cultures of *Anabaena* sp. strain PCC 7120 and the *hetR* mutant strains were grown to an approximate optical density of 0.4 at 750 nm in BG-11 medium, which contains nitrate, a fixed form of nitrogen. For one set of cultures, the culture medium was replaced with fresh BG-11, and replaced thereafter every 48 h with BG-11_0, which lacks fixed nitrogen. For the other set of

cultures, PatS-5 was included in the medium at a concentration of 1 μM. The percentage of 500 cells that were heterocysts was determined microscopically and recorded after each change of medium. Reported values are the average of three replicates with one standard deviation. Conditions for photomicroscopy were as described previously.[33]

Cloning, Overexpression, and Purification of Recombinant Soluble HetR. The *hetR* gene was PCR amplified from genomic DNA of *Anabaena* sp. PCC 7120 using the forward primer 5′-ATCGATCGCATATGAGTAACGACATCGATCTGATC-3′ and the reverse primer 5′-TGACTCTCGAGCTAATCTTCTTTTCTACCAAACACC-3′, cloned into pET28b (Novagen) at Nde I and Xho I sites with an N-terminal 6xHis tag including a thrombin cleavage site, then transformed into competent cells of the cloning host *E. coli* DH5α. Information regarding preparation of *hetR* mutants can be found in Supporting Information Table S3. All mutants were generated using the QuickChange II XL site-directed mutagenesis kit (Stratagene) and their DNA sequences confirmed by capillary electrophoresis based sequencing at the Miami University Center for Bioinformatics and Functional Genomics. HetR 250-256C mutants were generated using the C48A mutant plasmid as the DNA template. Correctly mutated 250-256C plasmids were transformed into BL21(DE3) competent cells containing the pGroESL vector to assist in proper protein folding.[45] The plasmid construct was isolated using a Wizard Plus Miniprep kit (Promega) and transformed into competent cells of the expression host BL21(DE3) (Novagen). The *hetR*-containing *E. coli* clone was grown at 37 °C with 250 rpm shaking to an OD_{600} of 0.6−0.9 in 1 L of LB-Miller broth supplemented with 30 μg/mL kanamycin. Protein expression was induced by addition of 0.25 mM isopropyl β-D-1-thiogalactopyranoside at 18 °C overnight. Cells were harvested and stored at −80 °C for later use. Thawed cells were resuspended in 25 mL of lysis buffer [1 M NaCl, 10% (w/v) glycerol, 10 mM Tris, pH 7.8] followed by four passes through a French Pressure Cell Press (Thermo Fisher). Cell lysates were centrifuged at 24 000*g* for 20 min. The supernatant was loaded onto a 10 mL Ni-NTA affinity column (Qiagen) and washed with 50 mL of wash buffer [1 M NaCl, 10% (w/v) glycerol, 10 mM Tris, pH 7.8] followed by a second wash with pre-elution buffer [1 M NaCl, 10% (w/v) glycerol, 10 mM Tris, pH 7.8, 30 mM imidazole]. Soluble His tagged protein was eluted from the Ni-NTA column with elution buffer [1 M NaCl, 10% (w/v) glycerol, 10 mM Tris, pH 7.8, 300 mM imidazole] and concentrated with an Amicon Ultra (Millipore) to a concentration of 15 mg/mL as determined by the Bradford assay (Thermo Scientific). Concentrated protein solutions were further purified and analyzed on a Pharmacia Superdex200 HiLoad size exclusion column equilibrated with buffer containing 1 M NaCl, 10% (w/v) glycerol, 10 mM Tris, pH 7.8, and 300 mM imidazole using a flow rate of 1 mL/min. The mutants co-expressed with the GroESL chaperone were also supplemented with 30 μg/mL chloramphenicol during expression. Circular dichroism spectra of HetR in the absence of phenylmethanesulfonylfluoride protease inhibitor did not change with the buffer and solution conditions used in our experiments following incubation at 37 °C for 24 h indicating no loss of structure or change in the secondary structure composition of the protein due to autoproteolytic activity, which has been reported by Zhou et al.[30,31] Calcium ion concentrations in these solutions were on the order of 50 μM as determined by inductively coupled plasma atomic emission spectroscopy.

DNA Binding Assays. Electrophoretic mobility shift assays were performed using 1.8% agarose gels. Agarose gel electrophoresis experiments used buffer containing 0.2 μg/mL ethidium bromide (Fisher) run at 80 mAmp for 1 h in TAE buffer. DNA binding reactions were incubated for 10 min at 22 °C prior to electrophoresis. Images were generated using an Alpha Innotech camera and Alpha Imager software. The individual strands of the 29 base pair inverted repeat upstream DNA fragment were synthesized (250 nmol scale synthesis for each strand) and HPLC purified (for determining HetR binding stoichiometry), or for all other experiments, synthesized at a 25 nmol scale with standard desalting, by Integrated DNA Technologies (Coralville, IA). The complementary oligonucleotides, forward 5′-GTAGGCGAGGGGTCTAACCCCTCATTACC-3′ and reverse 5′-GGTAATGAGGGGTTAGACCCCTCGCCTAC-3′, were annealed by suspending equivalent stoichiometric amounts at 200 μM in the same buffer used to prepare HetR solutions, heated to 85 °C, and then allowed to cool slowly to room temperature. PatS-5 (RGSGR) peptide was custom synthesized and purified by A & A Laboratories LLC (San Diego, CA), and PolyG (GGGGG) peptide was synthesized and purified by Peptide2.0 (Chantilly, VA), both on a 10 mg scale. PatS-5 was suspended in 100% nanopure H_2O to stock 10 mM concentrations. PolyG was suspended in 100% acetonitrile to a stock 10 mM concentration.

Circular Dichroism Spectroscopy. Circular dichroism spectra were obtained on a Jasco model J-810 spectropolarimeter. Measurements were obtained using 300 μL of approximately 15 μM recombinant HetR at 25 °C using a quartz cell of 1 mm path length. All reported circular dichroism spectra were the result of 10 averaged scans from 200 to 250 nm. Jasco Spectra Analysis software was used to generate the plots of molar ellipticity versus wavelength.

Site-Directed Spin Labeling. The nitroxide spin radical (1-oxyl-2,2,5,5-tetramethyl-pyrrolin-3-yl)methyl methanethiosulfonate (MTSL) (Toronto Research Chemicals, Inc.) was dissolved in 50% methanol to a stock concentration of 35 mM. HetR 250-256C mutants were spin-labeled using a 2-fold molar excess of MTSL at 22 °C in the dark overnight with gentle shaking. Excess label was removed (confirmed using CW-EPR) by size exclusion chromatography using an analytical grade Pharmacia Superdex200 10/300 GL column.

Preparation of Samples for EPR Spectroscopy. Spin-labeled HetR proteins were concentrated to 100 μM. For CW-EPR experiments, 30 μL of protein solution was drawn into 1.1 mm internal diameter (1.6 mm external diameter) quartz capillaries. The capillary tubes containing the samples were then placed into 3 mm internal diameter quartz EPR tubes and inserted into the instrument microwave cavity. For pulsed EPR DEER experiments, a cryoprotectant was added to the samples (samples were brought to a final concentration of 30% glycerol) and then 8 μL of the cryoprotected protein solutions was drawn into 1.1 mm internal diameter (1.6 mm external diameter) quartz capillaries. The capillary tubes containing the samples were frozen in liquid nitrogen and then inserted into the resonator for data collection. For DEER experiments involving samples containing DNA, the DNA concentration was 100 μM.

EPR Spectroscopy. EPR spectra were collected at the Ohio Advanced EPR Laboratory. CW-EPR spectra were collected at X-band on a Bruker EMX CW-EPR spectrometer

using an ER041xG microwave bridge and ER4119-HS cavity coupled with a BVT 3000 nitrogen gas temperature controller (temperature stability ±0.2 K). CW-EPR spectra were collected by signal averaging 15 42-s field scans with a center field of 3370 G and sweep width of 100 G, microwave frequency of 9.5 GHz, modulation frequency of 100 kHz, modulation amplitude of 1 G, and microwave power of 1 mW at 298 K. DEER data were collected using a Bruker ELEXSYS E580 spectrometer equipped with a SuperQ-FT pulse Q-band system and EN5107D2 resonator. DEER data were collected at Q-band with a probe frequency of 34.174 GHz and a pump frequency of 34.235 GHz, a probe pulse width of 20/40 ns, a pump pulse width of 48 ns, shot repetition time of 499.8 μs, 100 echoes/point, and 2-step phase cycling at 80 K collected out to 2 ns.

EPR Spectral Simulations. Qualitative analysis of spin-label mobility was obtained from simulations of the CW-EPR line shapes to extract best-fit values of the inverse line-width of the central resonance line (ΔH_0^{-1}) and the components of the diffusion tensor (**R**) required to reproduce the observed averaging of the hyperfine interaction tensor. The line-width of central resonance line was calculated by measuring central peak-to-peak magnetic field from the first derivative spectrum. Simulations were performed in Matlab using a nonlinear least-squares data analysis program developed by Budil et al.[46,47] The three components of electronic Zeeman interaction tensors (g_{xx}, g_{yy}, and g_{zz}) and hyperfine interaction tensors (A_{xx}, A_{yy}, and A_{zz}) were optimized using the spectrum of HetR 256C, which was characteristic of a spin label approaching the rigid limit. This spectrum provided well-defined features to constrain the **A** and **g** tensors to account for the polarity of the local environment of the MTSL nitroxide spin label.[48,49] The **A** and **g** tensors were held constant for all remaining simulations and it was assumed that remaining differences in spectra were due to differential motion of the MTSL spin label. The three components of the rotational diffusion tensor (R_{xx}, R_{yy}, and R_{zz}) were varied during fitting. The best-fit components of the tensor were averaged to report the overall rate of diffusion ($R_{iso} = 1/3(R_{xx} + R_{yy} + R_{zz})$).[50] EPR spectra of HetR 252C in the presence of PatS-5 consisted of a sum of free and Pats-5 bound species. In this case, a two-site fit was used to account for free and bound states. Best-fit diffusion tensors for each species in the mixture were determined using a Brownian diffusion model. The percentage contribution of each motional component to the overall spectrum was obtained for each sample. DEER data was simulated using DEER Data Analysis 2009.[51] The distance distributions $P(r)$ were obtained by Tikhonov regularization[52] in the distance domain, incorporating the constraint $P(r) > 0$. The regularization parameter was adjusted to obtain the realistic resolution.

Molecular Dynamics Simulations. The atomic coordinates for the HetR crystal structure (PDB ID: 3QOE) from *Fischerella* were downloaded from the Protein Data Bank and used to generate the structures of various spin-labeled HetR constructs with the Nanoscale Molecular Dynamics (NAMD) program.[53] The C48A and 250-256C mutations were created using the molecular graphics software VMD.[54] The nitroxide spin-probe MTSL was attached using CHARMM force field topology files incorporated into NAMD. The modified protein assembly was solvated into a spherical water environment and further equilibrated and minimized by running NAMD simulations at room temperature using CHARMM force field parameters. The distance distribution for the 252C mutants was predicted with rotamer library modeling of MTSL conformations using Multiscale modeling of macromolecular systems (MMM version 2010).[55]

Isothermal Titration Calorimetry (ITC). ITC measurements were performed at 25 °C with a VP-ITC titration calorimeter (Microcal, Northampton, MA). Size-exclusion-chromatography purified HetR samples were dialyzed for 18 h at 4 °C against the reference buffer: 1 M NaCl, 10% glycerol, 300 mM imidazole, 10 mM Tris, pH 7.8. HetR was then diluted to a final concentration of 5 μM for experiments. PatS-5 peptide was diluted into the reference buffer to a final concentration of 100 μM. The titrations were performed in triplicate using a total of 36 injections of PatS-5 peptide for each titration as follows: one 4-μL injection followed by 35 8-μL injections. For each titration, 0.60 mL of 100 μM PatS-5 peptide was loaded into the injection syringe. Blank titrations of PatS-5 solutions into reference buffer were performed to correct for the heats of dilution of PatS-5, which were found to be insignificant. Following the blank experiments, a 1.46 mL sample of HetR was degassed and loaded into the sample cell from the 5 μM prepared stock for each titration. The resulting titration curves were deconvoluted and fit using a one binding site model with the ORIGIN for ITC software package (Microcal, Piscataway, NJ).

RESULTS

Conservative Substitutions at HetR Residues 250–256 Affect Heterocyst Formation and Sensitivity to PatS-5. As part of a mutagenesis study designed to identify residues of HetR required for function, an allele of *hetR* coding for an E254G substitution was found to cause differentiation into heterocysts of essentially all cells containing a multicopy plasmid carrying the mutant gene.[33] Introduction of a plasmid bearing the *hetR(E254G)* allele under the control of the native *hetR* promoter by conjugation resulted in no viable trans-conjugants. To limit expression of the *hetR(E254G)* allele, the wild-type promoter region was replaced with that of the copper-inducible *petE* promoter and the plasmid was introduced into PCC 7120. Limited growth of a small number of transconjugants on solid BG-11 medium containing ammonia and lacking copper was observed. The resulting colonies lacked the green color of colonies of the wild type, were composed primarily of heterocysts, and showed little to no growth in liquid culture (data not shown). By comparison, a strain with P*petE* driving transcription of the wild-type allele of *hetR* in place of the *hetR(E254G)* allele under the same conditions differentiated less than 1% heterocysts. Replacement of the wild-type promoter region with a second promoter, that of *nirA*, from which transcription is repressed in ammonia and induced in nitrate or in the absence of fixed nitrogen,[56] permitted the growth of filaments on solid and liquid BG-11 medium with ammonia replacing nitrate as the nitrogen source. Apparently, there is tighter on−off control of transcription with the *nir* promoter than with *petE* in our hands. Transfer of filaments to BG-11 with nitrate or lacking a fixed source of nitrogen resulted in the differentiation of greater than 90% of cells into heterocysts. By comparison, a strain with P*nir* driving transcription of the wild-type allele of *hetR* in place of the *hetR(E254G)* allele under the same conditions differentiated about 30% heterocysts (data not shown). When the native copy of *hetR* in PCC 7120 was replaced with an allele encoding the E254G substitution, about 25% of cells in the resulting strain were heterocysts 48 h after induction. The phenotype of this strain was indistinguishable from that of a strain with a copy of

hetR encoding the conservative E254D substitution, which is discussed in more detail below.

Differentiation of nearly all cells of a filament has been observed when both *patS* and *hetN* are inactivated simultaneously or when an allele of *hetR* encoding protein less sensitive to both inhibitors is overexpressed ectopically and the mutant strains are grown in the absence of combined nitrogen.[35,57] To determine if the conservative E254D substitution also resulted in an overactive allele of HetR and if residues in the region of E254 were involved in the response of HetR to PatS-5, alleles of HetR encoding individual conservative substitutions at residues R250–D256 were used to substitute *hetR* by allelic replacement in PCC 7120 (see Supporting Information Table S1). Filaments of strains with alleles encoding R250K, E253D, E254D, L255V, and D256E substitutions consisted of about 14–48% heterocysts, and the presence or absence of fixed nitrogen in the medium had little effect on differentiation by an individual strain. By comparison, about 9% of cells in filaments of PCC 7120 were heterocysts in a medium that lacked fixed nitrogen, and about 1% when fixed nitrogen was present. Conversely, A251G and L252V substitutions prevented or reduced differentiation, respectively (Figure 1). Strains that differentiated an increased number of heterocysts were also less sensitive to PatS-5. Addition of PatS-5 to the growth medium prevented differentiation of heterocysts by the wild-type strain, PCC 7120.[25] In contrast, 8–25% of cells in filaments of strains with alleles encoding R250K, E253D, E254D, L255V, and D256E substitutions were heterocysts in a medium that contained PatS-5 at a concentration of 1 μM (Figure 1). As expected, PCC 7120 lacked heterocysts under the same conditions. Taken together, these results suggested that residues R250, E253, E254, L255, and D256 of HetR were involved in sensitivity to PatS-dependent signals *in vivo*.

Evidence for Direct Binding of PatS-5 to HetR. The previous experiments pointed to amino acids at the C-terminus as being important for HetR sensitivity to PatS. Guided by these *in vivo* observations, we designed *in vitro* experiments to test the hypothesis that PatS-5 binds to HetR in the vicinity of amino acids 250–256. Initially, we characterized the mobility and secondary structural environment of these amino acids using a combination of site-directed spin labeling and continuous wave (CW) EPR spectroscopy to provide a baseline for PatS-5 binding studies. We then used these techniques to determine how the mobility of these residues were affected by addition of PatS-5 since CW-EPR spectra of MTSL spin-labeled proteins can be affected by interactions with other proteins, peptides, or small molecules.[58−62] To enable this approach, it was necessary to employ site-specific mutagenesis and nitroxide spin labeling,[63] whereby amino acids 250–256 were individually mutated to cysteine and then labeled with the stable nitroxide free radical (1-oxyl-2,2,5,5-tetramethyl-pyrrolin-3-yl)methyl methanethiosulfonate (MTSL). To ensure that MTSL labeling occurred only at one position on the protein, this introduced cysteine needed to be the only cysteine in the protein. Therefore, the HetR used to generate CW-EPR spectra had a C48A substitution to remove the naturally occurring cysteine in addition to substituting amino acids 250–256 individually with cysteine. The C48A substituted protein resembled the unmodified protein in its DNA binding capability and its sensitivity to PatS-5 (see below). The CW-EPR spectrum of each MTSL-labeled HetR mutant is shown in Figure 2. Control CW spectra of each MTSL spin-labeled

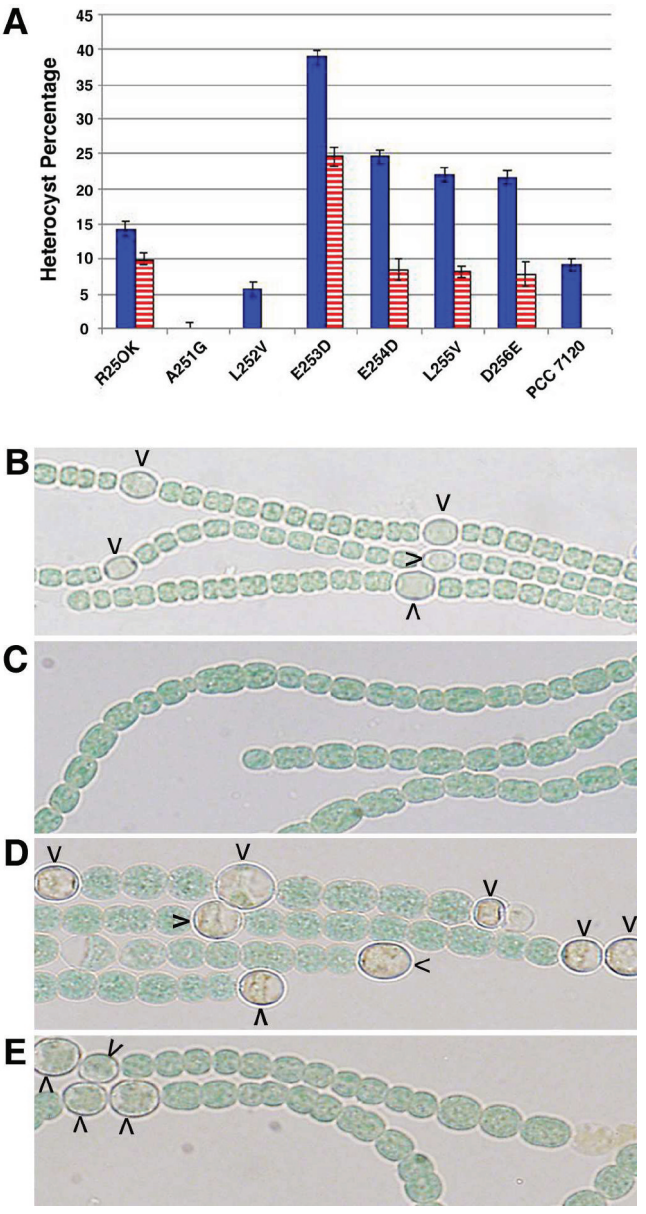

Figure 1. Sensitivity to PatS-5 of strains with mutant alleles of *hetR*. (A) Bar graph of the percentage of cells that are heterocysts in the wild-type strain (PCC 7120) and strains with an allele of *hetR* encoding the indicated amino-acid substitution 96 h after removal of combined nitrogen with (red-striped bars) or without (solid blue bars) the addition of PatS-5 to the medium. Values represent the average of 500 cells from three independent cultures. Strain PCC 7120 (B and C) and UHM167, which contained an allele of *hetR* encoding an E254D substitution (D and E), 96 h after removal of combined nitrogen without (B and D) or with (C and E) the addition of PatS-5 to the medium. Carets indicate heterocysts.

mutant were recorded at 100 μM protein, a concentration unlikely to exist in cells but required for measurement of the CW-EPR spectra. CW-EPR spectra were collected for each mutant after each titration with 100 μM, 200 μM, 500 μM, and 1 mM PatS-5. Simulations enabled determination of **g**-, **A**-, and **R**-tensor parameters (Table S4). CW-EPR spectra of MTSL labeled at positions R250C and L252C exhibited significant conformational averaging based on their central resonance line widths and isotropic rotational diffusion rates (ΔH_o = 2.03 and 3.45 G, and R_{iso} = 5.37 × 10^7 and 63.39 × 10^6 s^{-1}, respectively)

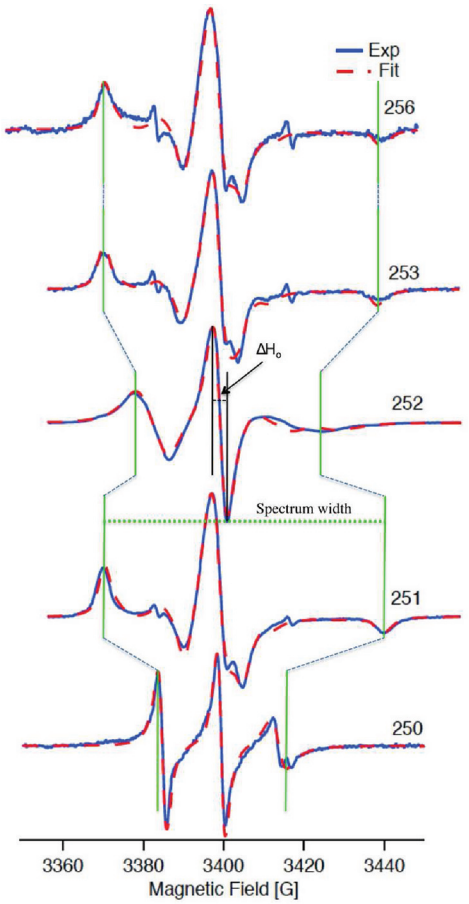

Figure 2. Room temperature X-band CW-EPR spectra showing variations in spin label mobility for HetR mutants in the range 250–256. The amino acid position of the MTSL label is indicated above each spectrum. The solid blue line indicates experimental data and the red dashed line is the best-fit simulation of the data. Simulation parameters are included in Supporting Information Table S4.

indicating these residues likely occurred either on surface exposed helices or surface exposed loops.[61,64,65] MTSL at the A251C, E253C, and D256C positions were less mobile with time-scales of motion too slow to cause motional averaging of the hyperfine interaction tensor (ΔH_o values in the range 5.85–7.70 G and R_{iso} values in the range of 3.47×10^5 to 3.98×10^5 s^{-1}) indicating that they likely resided either at helix–helix contacts or in buried locations within the protein.[61,64,65] The E254C and L255C mutants were difficult to label, exhibited intrinsic protein instability and aggregation, gradually precipitated over time, and produced poor EPR spectra, indicating that mutations at these sites disrupted the local protein structure.

The recently released HetR crystal structure from *Fischerella* (PDB ID: 3QOE,[43]) was used to examine the structural context of the MTSL spin-label in each HetR cysteine mutant. The atomic coordinates for the structure were downloaded from the Protein Data Bank and analyzed using the program VMD[54] in order to generate the C48A mutation, followed by individual R250C–E256C cysteine mutations. Following substitutions, MTSL groups were engineered onto the side chains, attached via the disulfide linkage to the free sulfhydryl of cysteine using NAMD,[53] and then simulated to achieve a local energy minimization. The resulting structures are shown in Figure 3 and the general location of amino acids 250–256 can be seen in Figure 3A. A clear correspondence was evident between the location of each spin label and the magnitude of the conformational mobility based on the inspection and simulation of the CW-EPR spectra. For example, the 250C mutant exhibited a highly motionally averaged EPR spectrum (Figure 2) that was consistent with the location of residue 250 on the surface of the protein (Figure 3B). The 251C mutant displayed an EPR spectrum devoid of motional averaging and the spin label appeared buried in the model (Figure 3C). The 252C mutant exhibited significant motional averaging, consistent with the location of the spin label on the surface of the protein (Figure 3D). Likewise, the EPR spectra of the 253C and 256C mutants showed no signs of motional averaging consistent with the buried nature of the spin label in the models (Figure 3E,H). Models of 254C and 255C mutants are included in Figure 3F,G for the sake of completeness.

The CW-EPR spectrum of HetR spin-labeled at 252C changed dramatically after addition of PatS-5 (Figure 4), going from a distinctly motionally averaged spectrum in the absence of PatS-5 to a spectrum that showed no evidence of motional averaging with a 10-fold molar excess of PatS-5, indicating substantial quenching of the conformational dynamics of the MTSL nitroxide electron radical upon addition of PatS-5. These observations provided clear evidence for direct binding between HetR and PatS-5. At PatS-5 to HetR-252C ratios <10:1, a mixture of free and bound states in slow exchange was evident and the EPR spectra could be explained as a sum of spectra for free HetR mutant and HetR mutant bound to PatS-5. Simulations of the CW-EPR spectra of the MTSL-labeled HetR-252C mutant enabled determination of the change in the overall diffusion constant for spin-label motion after binding to PatS-5, indicating almost an order of magnitude reduction in the diffusion rate in the bound state ($R_{iso} = 4.17 \times 10^6$ s^{-1} in the free state compared to an upper limit of $R_{iso} = 8.32 \times 10^5$ s^{-1} in the bound state; simulation parameters are in Supporting Information Table S4). Quenching of the spin-label motion indicated either a proximal interaction with PatS-5 binding nearby, but not necessarily at, amino acid 252, or a distal interaction in which PatS-5 could bind away from the spin label, but the spin label motion could be quenched due to a tertiary or quaternary structural change that caused restriction of the spin label motion at amino acid 252.

Evidence for PatS-5 Binding to the Dimer form of HetR. The pulsed EPR DEER experiment[66,67] can be used to measure long-range distances (from 20 to 70 Å) between spin labels in large proteins.[68,69] Here, DEER EPR experiments were used (1) to measure the intermolecular distance across the HetR homodimer, (2) to determine if PatS binding caused a change in the quaternary structure of the HetR dimer, and (3) to determine if PatS-5 binding disrupted the HetR dimer. DEER data was initially collected on the MTSL-labeled 252C HetR mutant. The time-domain DEER signal (Figure 5A) had an excellent signal-to-noise ratio and exhibited a strong modulation indicating substantial dipolar coupling between the two MTSL spin labels across the dimer. Fourier transform of the time domain DEER modulation produced a dipolar spectrum with well-defined features (Figure 5B). Simulations of the time-domain DEER data produced a clear peak maximum in the distance distribution indicating that the distance between the MTSL spin labels in each monomer was 2.7 nm (Figure 5C). Observation of a DEER signal in the MTSL spin-labeled 252C mutant (which contained the C48A mutation) confirmed that C48 was not necessary for HetR dimer formation, since no

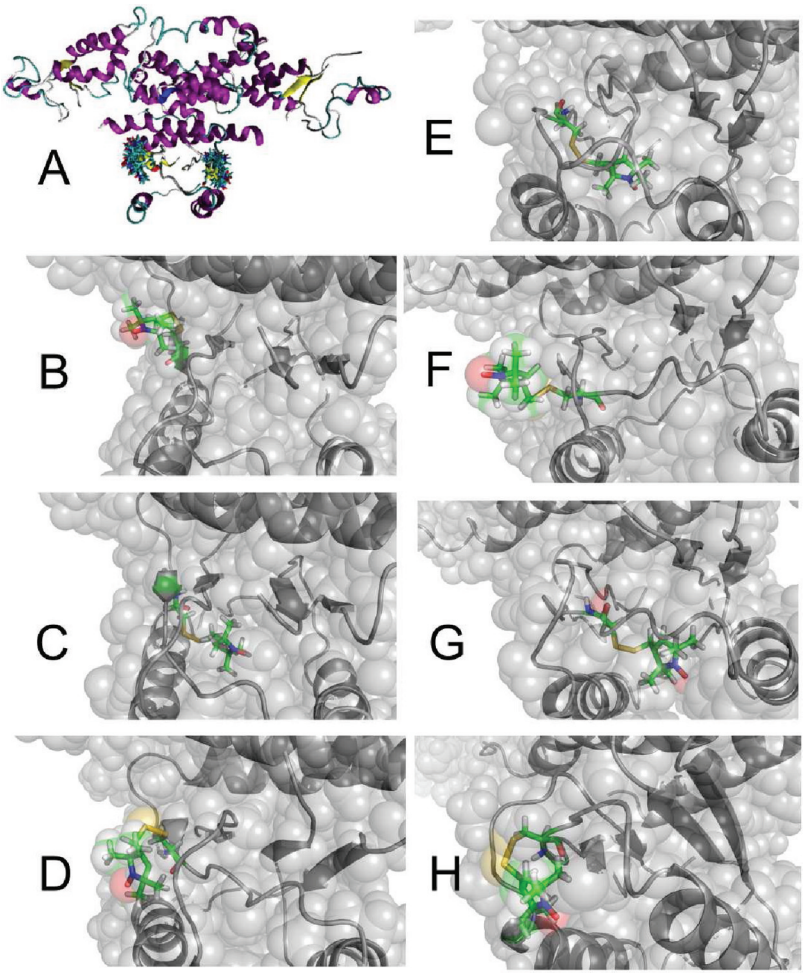

Figure 3. (A) Crystal structure of the HetR homodimer (PDB ID: 3QOE,[43]) from *Fischerella* with the general location of residues 250−256 depicted by stick representation, which were rendered using Pymol molecular visualization software (The PyMOL Molecular Graphics System, Version 1.3, Schrödinger, LLC.). Space filling representation of the MTSL group in HetR mutant (B) 250C, (C) 251C, (D) 252C, (E) 253C, (F) 254C, (G) 255C, and (H) 256C.

DEER signal would be detectable if the HetR mutant existed as a monomer in solution. In the presence of a 10-fold excess of PatS-5, the DEER signal was virtually unchanged compared to the HetR alone sample, demonstrating that PatS-5 binds to HetR without disrupting the HetR dimer. Furthermore, the distance between the spin labels, measured to be 2.6 nm in the presence of bound PatS-5, was the same within the uncertainty of the measurement as the distance measured for HetR in the absence of bound PatS-5, indicating that HetR binding to PatS-5 did not cause a structural rearrangement that resulted in a change in the distance between the two spin-labeled 252C residues in the HetR dimer. Furthermore, a DEER distance of 2.7 nm was measured when HetR 252C was bound to the 29 base pair *hetP* DNA fragment, also indicating that the HetR dimer also did not undergo a structural rearrangement that changed the distance between the two 252C residues in the HetR dimer upon DNA binding. The atomic coordinates of the crystal structure of HetR from *Fischerella* (PDB ID: 3QOE,[43]) were used to independently measure the distance across the HetR dimer between residue 252 in the two chains (Figure 6). The crystal structure was modified as discussed in the Materials and Methods to create the 252C mutant modified by the MTSL spin label. The resulting modified structure was subjected to molecular dynamics simulation to create an ensemble of structures, which are depicted in Figure 6A. Distance measurements between the nitroxide groups of the 252C-MTSL modified mutant revealed an average N−N distance of 26.5 Å and an average O−O distance of 27.9 Å (Figure 6B), consistent with our observed DEER distance of 27 Å.

Characterization of Binding of HetR to a 29 bp Inverted Repeat Containing DNA Sequence Upstream of *hetP*. HetR was recently shown to bind tightly to a 29 bp region upstream of the *hetP* gene containing the inverted repeat sequence 5′-GAGGGGTCTAACCCCTC-3′.[70] Indeed, HetR appears to bind more tightly to this upstream *hetP* DNA sequence than to any previously used DNA substrate reported in the literature, and thus, enabled us to investigate the stoichiometry of HetR binding to DNA. At a HetR to DNA ratio of 3:1, the majority of the DNA was shifted and approximately half of the DNA was shifted at between 2:1 and 3:1 (Figure 7). This data is consistent with HetR binding the DNA with a 2:1 stoichiometry, since the extent of completion of the gel shift depends on the dissociation constant, K_d. All these data taken together, along with the fact that most prokaryotic transcription factors bind inverted repeat DNA sequences as homodimers,[71−73] suggested that HetR bound this single inverted-repeat containing upstream *hetP* DNA

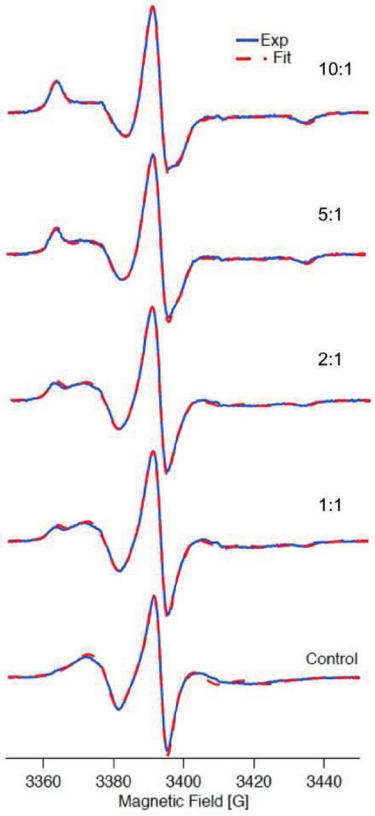

Figure 4. CW-EPR spectra indicating direct binding between HetR and PatS-5. The MTSL-labeled 252C HetR mutant was titrated with PatS-5 and monitored by CW X-band EPR spectroscopy at room temperature. The control spectrum is shown at the bottom. For the remaining spectra, the ratio of PatS-5 to HetR-252C (indicated above each spectrum) increases from bottom to top in the stack. The solid blue line indicates experimental data and the red dashed line is the best-fit simulation of the data. Parameters for the EPR spectral simulations are included in Supporting Information Table S4.

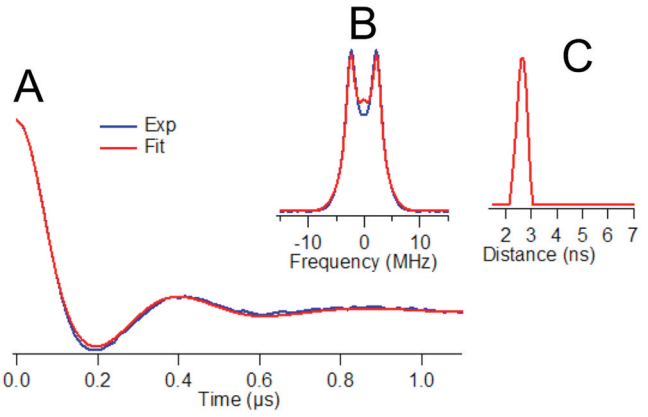

Figure 5. DEER data for 252C HetR mutant. (A) The time-domain DEER signal; (B) the frequency spectrum resulting from the Fourier transform of the time-domain data; (C) the best fit of the distance distribution that explains the DEER data using a Tikhonov regularization fitting procedure.

sequence as a homodimer. Interestingly, at HetR to DNA ratios greater than 4:1, a supershifted species was also present (Figure 7) possibly caused by two HetR homodimers binding to a single 29 base pair DNA molecule. It appears that the supershifted species was not caused by nonspecific DNA

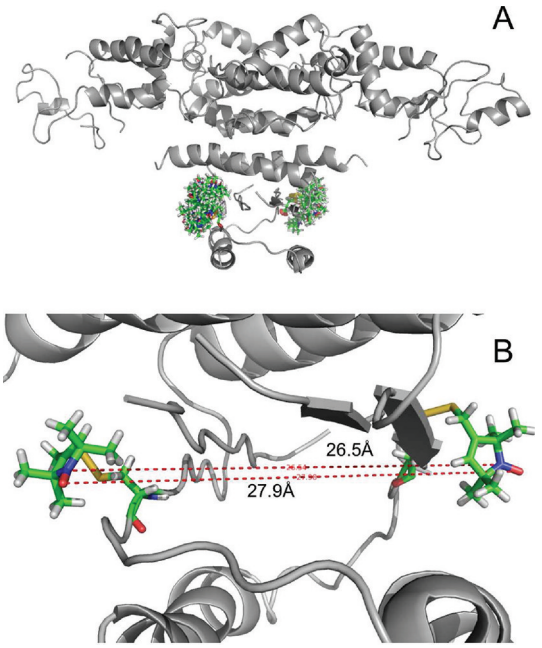

Figure 6. (A) Superposition of an ensemble of structures of MTSL modified 252C HetR mutant generated by molecular dynamics simulation starting from the crystal structure of the HetR homodimer (PDB ID: 3QOE,[43]) from *Fischerella* as described in the Materials and Methods. (B) Representation of the average distance between the nitroxide groups of the 252C-MTSL HetR mutant revealed an average N−N distance of 26.5 Å and an average O−O distance of 27.9 Å.

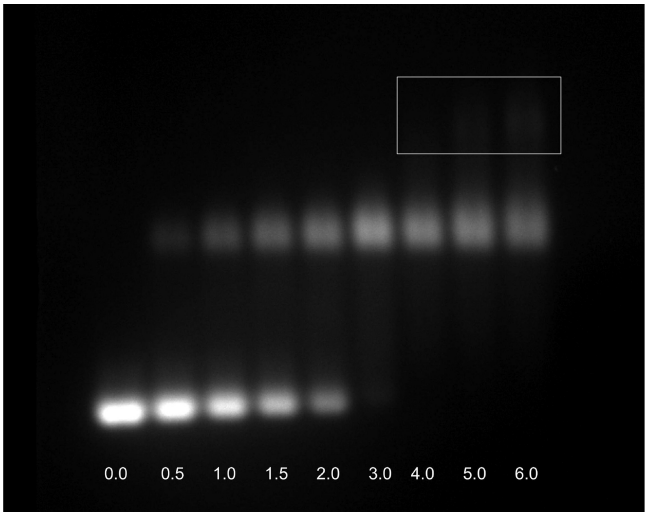

Figure 7. EMSA showing binding of HetR to the 29 base pair inverted repeat containing upstream *hetP* DNA fragment. The ratio of HetR to DNA increases from left to right. The resulting completeness of shifted DNA was used to assess the stoichiometry of binding between HetR and DNA as one molecule of HetR dimer per double stranded DNA molecule. The box contains the supershifted bands observed at high HetR to DNA ratios.

binding since no supershifted species was observed when HetR was mixed with negative control DNA (taken from the human interleuken−2 receptor alpha chain gene promoter PRRII) of the same length and at 100:1 ratio of HetR to DNA (data not shown). The amount of supershifted species depended on the amount of NaCl in solution with the largest ratio of DNA in the

dx.doi.org/10.1021/bi201226e | *Biochemistry* 2011, 50, 9212−9224

supershifted band compared to the shifted band being observed when using 0.5 M NaCl in the solution (data not shown).

Sensitivity of the HetR–DNA Complex to PatS-5. The strong interaction between HetR and DNA from the *hetP* promoter region permitted assessment of the PatS-5 to HetR ratios required to disrupt HetR binding to DNA. In gel shift assays, we found that PatS-5 completely disrupted the supershifted species at a substoichiometric ratio of 0.5:1 PatS-5 to HetR monomer and the shifted species was completely disrupted at a 10:1 ratio of PatS-5 to HetR (Figure 8). When

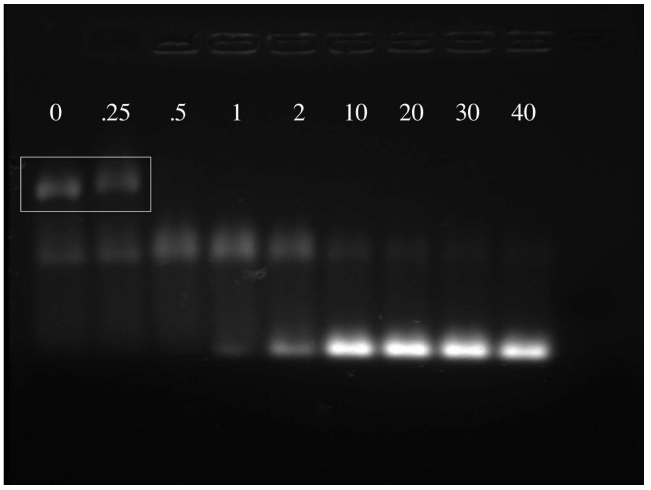

Figure 8. Agarose gel shift analysis of PatS-5 disruption of complex formation between HetR and the 29 base pair inverted repeat containing upstream *hetP* DNA fragment. The numbers above each lane indicate the ratio of PatS-5 to HetR monomer. The ratio of HetR to DNA was held constant at 4:1 in each lane. The DNA concentration was 12.5 μM and the HetR concentration was 50 μM. The box indicates the supershifted bands.

PatS-5 was titrated into a solution of the MTSL-labeled HetR 252C–DNA complex, the CW-EPR spectra were the same as HetR plus PatS-5 alone (Supporting Information Figure S1 and Table S4). This result was consistent with the gel shift assay showing that the HetR–DNA interaction was disrupted when HetR bound to PatS-5. In other words, in a solution containing HetR, PatS-5, and DNA, only a complex of HetR and PatS-5 would exist and the DNA would be free in solution.

Similarity of HetR and HetR-C48A. As mentioned above, HetR containing a C48A substitution was used in the CW-EPR work that showed binding of PatS-5. It was therefore important to examine whether C48A-substituted HetR behaved similarly to wild-type protein. Huang et al.[29] previously reported that HetR residue C48 was required for both dimer formation and DNA binding. Here, size exclusion chromatography analysis of HetR-C48A showed that it eluted as a dimer identically to wild-type HetR indicating that the proposed intermolecular cysteine disulfide bond was not required for dimer formation (Supporting Information Figure S1). The DEER EPR data confirmed that the C48A HetR spin-labeled mutant existed as a dimer in solution (discussed above). Comparison of wild-type HetR and HetR-C48A using PAGE (Figure 9A) showed that the wild-type HetR exhibited a strong dimer band even under denaturing conditions (0.1% SDS in the protein buffer) and in the presence of 10 mM dithiothreitol, whereas the dimer band was almost completely gone in the C48A mutant under the same conditions. Huang et al.[29] reported that the dimer band

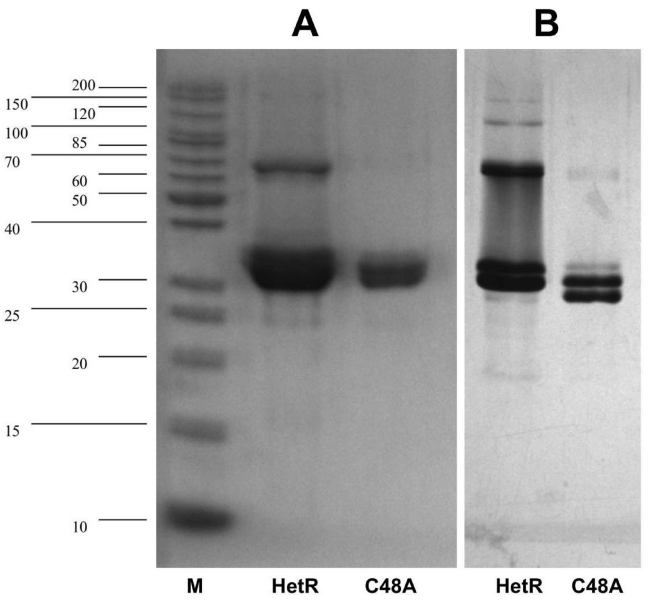

Figure 9. Polyacrylamide gel electrophoresis analysis of soluble-expressed purified recombinant HetR and C48A HetR mutant. (A) At 0.1% SDS and 10 mM dithiothreitol. Molecular weight markers (Fisher Bioreagents EZ-run *Rec* Protein Ladder) are indicated in units of kilodaltons (kDa) to the left of the lane marked M. (B) At 0.01% SDS and 10 mM dithiothreitol. Lanes are marked "HetR" for wild-type HetR and "C48A" for the C48A mutant of HetR.

was completely gone for the C48A HetR mutant in their SDS–PAGE analysis and concluded that HetR-C48A was unable to form dimers *in vitro*, that the HetR dimer was formed through a disulfide bond, and that Cys-48 was required for dimerization. We were, however, able to detect a dimer band for HetR-C48A under milder denaturing conditions using 0.01% SDS–PAGE (Figure 9B). Taken together with the size exclusion chromatography and DEER data, these results indicated that C48 was not required for dimer formation; however, the dimer still may be stabilized by an interchain disulfide bond. In addition, circular dichroism (CD) spectra of wild-type HetR and the C48A HetR mutant were identical and characteristic of a protein with predominantly α-helical secondary structure as indicated by distinct minima in molar ellipticity at 209 and 222 nm (wild-type HetR CD spectrum shown in Supporting Information Figure S2).

In addition to having the same physical characteristics as the wild-type protein, C48A substituted HetR behaved similarly to the wild-type HetR in gel shift assays. At the same concentrations as those described above, both shifted and supershifted species were observed; however, the supershifted band tended to be less prominent compared to that generated with wild-type HetR. The HetR-252C mutant also shifted DNA in the same manner as the C48A mutant of HetR (data not shown). When PatS-5 was included in the binding reactions, binding of the C48A HetR mutant to the 29 bp *hetP* promoter region was affected in a manner similar to that for the wild-type protein, suggesting that the C48A substitution does not affect binding of HetR to DNA or its interaction with PatS-5 peptide.

Determination of the Stoichiometry, Dissociation Constant, and Thermodynamic Parameters for Binding of PatS-5 to HetR. ITC is a highly sensitive biophysical technique for analyzing thermodynamics of molecular interactions. ITC can be used to study protein–protein or protein–

small molecule binding interactions and is capable of detecting heats of binding directly, without use of molecular labels or tags that might interfere with, or influence, binding.[74] Here, ITC was used to confirm direct binding of PatS-5 to HetR (Figure 10) and the integrated binding heats indicated a single exothermic binding event. A single binding site model was used to fit the binding curves, which allowed determination of the binding stoichiometry n, K_a (equal to $1/K_d$), and ΔH. The ΔG was determined from K_a, and ΔS was then calculated using the ΔG and ΔH values. The data indicated that one PatS-5 peptide bound to one HetR monomer, that is, two peptides bind per homodimer. Calculations of the thermodynamic parameters using a model for two noninteracting identical binding sites in a homodimeric protein should be equivalent to those obtained from calculations for a single peptide binding-site on a monomer.[75] PatS-5 was found to bind HetR with a mean K_d of 227 ± 23 nM, ΔG of −9.063 ± 0.059 kcal/mol, and n of 1.04 ± 0.01 sites, indicating a single tight exothermic binding interaction. PatS-5 binding to HetR exhibited a relatively large negative enthalpy (−8.337 ± 0.410 kcal/mol) and a positive entropy (2.44 ± 1.55 cal/(mol·deg)). Inspection of Table 1 shows that the binding affinity of HetR for PatS-5 was dominated by the change in enthalpy in comparison to the relatively small change (more than 10-fold smaller) in $T\Delta S$. This indicated that binding of PatS-5 to HetR was enthalpically, as opposed to entropically, driven. It is difficult to elucidate the relative contributions to PatS-5 binding; however, the relatively large negative enthalpy of binding is consistent with the formation of hydrogen bonds or ionic interactions, which are associated with relatively large negative contributions to enthalpy for ligands binding to proteins.[76−78] Collectively, the isothermal titration calorimetry data corroborate the EPR observations that PatS-5 binds directly to HetR in the absence of DNA.

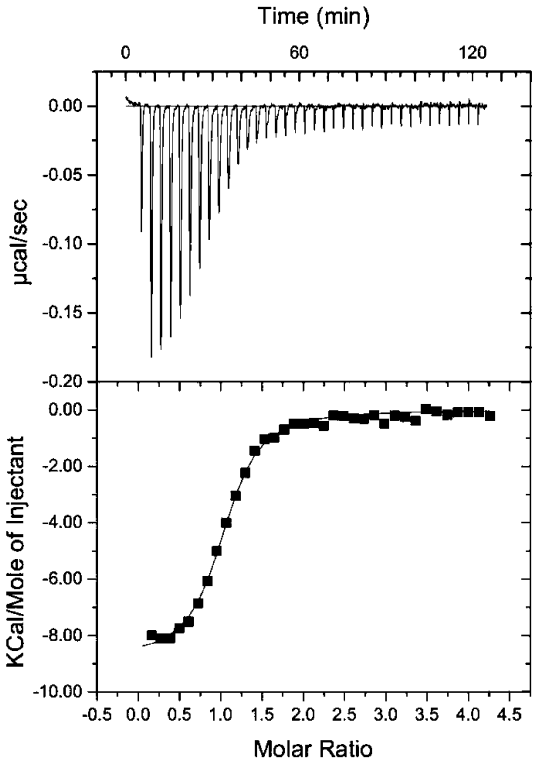

Figure 10. Representative ITC experiment for HetR binding to PatS-5. Experiments were performed in triplicate. Shown are the heat effects as a function of time (µcal/s) and the cumulative heat effects as a function of the molar ratio of PatS-5 peptide to HetR (kcal/mol). The solid line represents the fit to the experimental data.

DISCUSSION

Since the original report of PatS as a diffusible inhibitor of heterocyst differentiation,[25] the specific partners that interact directly in the process of PatS-dependent heterocyst regulation have been difficult to identify, both *in vitro* and *in vivo*. While multiple groups have demonstrated that the RGSGR carboxyl terminus of PatS is capable of inhibiting DNA binding of HetR to a region upstream from its own promoter *in vitro*,[29,33] and a R223W mutant of HetR has been shown to be insensitive to *in vivo* overexpression of both PatS and HetN,[35] all of these observations have provided only indirect evidence of binding between HetR and PatS. The specific partners that interact directly during PatS disruption of HetR binding to DNA and the direct molecular-level interactions that cause the loss of R223W HetR sensitivity to PatS have not been unambiguously elucidated with support of experimental data. Specifically with regards to the gel shift experiments, no experimental data has been reported in the literature to distinguish between the two following possibilities: (1) that PatS-5 displaces the DNA upon binding directly to HetR, or (2) that PatS-5 displaces HetR upon binding directly to the DNA. Resolving these issues has been impossible using traditional techniques used to observe direct intermolecular interactions, such as gel shift assays and size exclusion chromatography, because these techniques lack sufficient resolution to detect shifts in the migration of either the 70 kDa HetR dimer or the >20 kDa DNA fragments upon binding to the PatS-5 pentapeptide, which adds only about 0.6 kDa to the overall complex molecular weight. Moreover, PatS lacks any naturally occurring spectroscopic probe that could be used to detect binding between HetR and PatS-5.

In this manuscript, we report the first unequivocal experimental data that shows direct binding between HetR and PatS-5. Two different and independent techniques corroborated that PatS-5 bound directly to HetR, namely, EPR spectroscopy and isothermal titration calorimetry. The conclusion from the EPR experiments was based on the observation that the motion of the MTSL spin-label on the HetR 252C mutant was quenched upon titration with PatS-5 in the absence of any DNA in solution. This observation clearly indicated a direct binding interaction between the mutant spin-labeled HetR and PatS-5. However, these data did not unambiguously indicate that PatS-5 bound in the immediate vicinity of residue 252, since it is possible that PatS-5 could have bound to HetR in a site remote from residue 252 and

Table 1. Summary of Quantities Associated with HetR Binding to PatS-5 Peptide Derived from Isothermal Titration Calorimetry Experiments

peptide	n (no. of sites)	K_d (nM)	ΔG (kcal/mol)	ΔH (kcal/mol)	$T\Delta S$ (kcal/mol)
PatS-5	1.04 ± 0.01	227 ± 23	−9.063 ± 0.059	−8.337 ± 0.410	0.73 ± 0.46

dx.doi.org/10.1021/bi201226e | *Biochemistry* 2011, 50, 9212−9224

caused quenching of spin label motion through an allosteric effect or change in tertiary structure. However, given that *in vivo* experiments indicated that HetR residues 250−256 were critical for sensitivity to PatS-5, it would not be surprising if PatS-5 bound HetR in the C-terminal domain in the vicinity of amino acids 250−256. Besides demonstrating that PatS-5 bound directly to HetR, the DEER EPR experiments[79] also demonstrated that HetR persisted as a dimer even after binding PatS-5. The isothermal titration calorimetry data independently corroborated that PatS-5 bound directly to HetR, using the native HetR protein, without the mutation or MTSL spin-label required for the EPR experiments, and firmly established that the stoichiometry of binding was one PatS-5 peptide per HetR monomer, or said differently, two molecules of PatS-5 bind to each HetR dimer. By employing isothermal titration calorimetry, we were not only able to corroborate that PatS-5 bound directly to HetR in the absence of DNA, but we were also able to measure its dissociation constant and determine thermodynamic parameters, which indicated that binding of PatS-5 to HetR was enthalpically driven.

The high affinity of HetR for the 29 base pair inverted repeat containing upstream *hetP* DNA sequence enabled a semi-quantitative analysis of the stoichiometry of binding of HetR to this DNA fragment, which indicated HetR likely bound to this DNA in a 2:1 ratio, that is, HetR bound the inverted repeat containing upstream *hetP* DNA sequence as a homodimer. Finally, based on the determination that the shifted species was a 2:1 complex of HetR to DNA, we concluded that the supershifted complex possibly consisted of two HetR homodimers bound to a single *hetP* DNA sequence, which is consistent with the observation that the supershifted species was only detected when the ratio of HetR to DNA was greater than 4:1. Again, despite detecting the supershifted species, the biological relevance of this species, if any, remains to be determined.

The biophysical data was driven by the *in vivo* studies with mutant alleles of *hetR*. The phenotypes of strains with alleles of *hetR* encoding substitutions at residues R250, E253, E254, L255, and D256 were consistent with decreased sensitivity of the substituted HetR proteins to PatS- and HetN-dependent inhibitory signals. First, both *patS* and *hetN* null mutants as well as the strains with overactive alleles described here differentiated an increased number of heterocysts relative to that of the wild type, PCC 7120.[25,26] Second, a *patS* null mutant and the strains described here with overactive alleles differentiated heterocysts in the presence of a fixed source of nitrogen. And third, inactivation of both *patS* and *hetN* simultaneously resulted in the formation of a number of heterocysts in excess of that made by either of the individual mutants,[57] similar to the strains with alleles of *hetR* encoding E253D, E254D, L255V, and D256E substitutions.

■ ASSOCIATED CONTENT

Ⓢ Supporting Information

Figure S1 shows CW-EPR titrations of MTSL-252C labeled HetR with PatS-5 in the presence of DNA and titration with a poly-G5 control. Figures S2 and S3 show size exclusion chromatography and circular dichroism analysis of wild-type and C48A mutant HetR. Table S1 lists the strains and plasmids used in the study. Table S2 lists the primers used to generate chromosomal HetR mutants. Tables S3 lists the primers used to generate recombinant HetR mutants. Table S4 summarizes the parameters used to simulate the CW-EPR spectra described in the paper. This material is available free of charge via the Internet at http://pubs.acs.org.

■ AUTHOR INFORMATION

Corresponding Author

*Department of Chemistry and Biochemistry, Hughes Laboratories, Room 106, Miami University, 701 High Street, Oxford, OH 45056. E-mail: kennedm4@muohio.edu. Phone: 513-529-8267. Fax: 513-529-5715.

Funding

This work was supported in part by a grant from NSF (IOS-0919878) to S.M.C.

■ ACKNOWLEDGMENTS

The authors thank Professor Susan Barnum for providing the genomic DNA of *Anabaena* sp. strain PCC 7120 and Kelly Higa for insightful discussions. Bryan J. Glaenzer, Alisha N. Jones, and Andrea F. Schilling are acknowledged for contributing to early stages of characterization of soluble HetR.

■ REFERENCES

(1) Fritsch, F. (1904) Studies on cyanophyceae. *New Phytol. 3*, 85−96.

(2) Fogg, G. (1944) Growth and heterocyst production in Anabaena cylindrica Lemm. *New Phytol. 43*, 164−175.

(3) Fogg, G. (1949) Growth and heterocyst production in Anabaena Cylindrica Lemm. II In relation to carbon and nitrogen metabolism. *Ann. Bot. 13*, 241−259.

(4) Haselkorn, R. (1978) Heterocysts. *Ann. Rev. Plant Physiol. Plant Mol. Biol.*, 319−344.

(5) Adams, D. G., and Carr, N. G. (1981) The developmental biology of heterocyst and akinete formation in cyanobacteria. *Crit. Rev. Microbiol. 9*, 45−100.

(6) Wolk, C. P. (1996) Heterocyst formation. *Annu. Rev. Genet. 30*, 59−78.

(7) Adams, D. G. (2000) Heterocyst formation in cyanobacteria. *Curr. Opin. Microbiol. 3*, 618−624.

(8) Meeks, J. C., Elhai, J. (2002) Regulation of cellular differentiation in filamentous cyanobacteria in free-living and plant-associated symbiotic growth states. *Microbiol. Mol. Biol. Rev. 66*, 94−121; table of contents.

(9) Golden, J. W., and Yoon, H. S. (2003) Heterocyst development in Anabaena. *Curr. Opin. Microbiol. 6*, 557−563.

(10) El-Shehawy, R., and Kleiner, D. (2003) The mystique of irreversibility in cyanobacterial heterocyst formation: parallels to differentiation and senescence in eukaryotic cells. *Physiol. Plant.*, 49−55.

(11) Zhang, C. C., Laurent, S., Sakr, S., Peng, L., and Bédu, S. (2006) Heterocyst differentiation and pattern formation in cyanobacteria: a chorus of signals. *Mol. Microbiol. 59*, 367−375.

(12) Kumar, K., Mella-Herrera, R. A., and Golden, J. W. (2010) Cyanobacterial heterocysts. *Cold Spring Harbor Perspect. Biol. 2*, a000315.

(13) Brocks, J. J., Logan, G. A., Buick, R., and Summons, R. E. (1999) Archean molecular fossils and the early rise of eukaryotes. *Science 285*, 1033−1036.

(14) Tomitani, A., Knoll, A. H., Cavanaugh, C. M., and Ohno, T. (2006) The evolutionary diversification of cyanobacteria: molecular-phylogenetic and paleontological perspectives. *Proc. Natl. Acad. Sci. U.S.A. 103*, 5442−5447.

(15) Fay, P. (1992) Oxygen relations of nitrogen fixation in cyanobacteria. *Microbiol. Rev. 56*, 340−373.

(16) Gallon, J. (1992) Reconciling the incompatible: N2 fixation and O2. *New Phytol. 122*, 571−609.

(17) Haselkorn, R. (2008) Cell-cell communication in filamentous cyanobacteria. *Mol. Microbiol. 70*, 783−785.

(18) Fritsch, F. (1951) The heterocyst: a botanical enigma. *Proc. Linn. Soc. London 162*, 194−211.
(19) Wolk, C. P., and Quine, M. P. (1975) Formation of one-dimensional patterns by stochastic processes and by filamentous blue-green algae. *Dev. Biol. 46*, 370−382.
(20) Lambein, F., and Wolk, C. P. (1973) Structural studies on the glycolipids from the envelope of the heterocyst of Anabaena cylindrica. *Biochemistry 12*, 791−798.
(21) Khudyakov, I., and Wolk, C. P. (1997) hetC, a gene coding for a protein similar to bacterial ABC protein exporters, is involved in early regulation of heterocyst differentiation in Anabaena sp. strain PCC 7120. *J. Bacteriol. 179*, 6971−6978.
(22) Nicolaisen, K., Hahn, A., and Schleiff, E. (2009) The cell wall in heterocyst formation by Anabaena sp. PCC 7120. *J. Basic Microbiol. 49*, 5−24.
(23) Buikema, W. J., and Haselkorn, R. (1991) Characterization of a gene controlling heterocyst differentiation in the cyanobacterium Anabaena 7120. *Genes Dev. 5*, 321−330.
(24) Black, T. A., Cai, Y., and Wolk, C. P. (1993) Spatial expression and autoregulation of hetR, a gene involved in the control of heterocyst development in Anabaena. *Mol. Microbiol. 9*, 77−84.
(25) Yoon, H. S., and Golden, J. W. (1998) Heterocyst pattern formation controlled by a diffusible peptide. *Science 282*, 935−938.
(26) Callahan, S. M., and Buikema, W. J. (2001) The role of HetN in maintenance of the heterocyst pattern in Anabaena sp. PCC 7120. *Mol. Microbiol. 40*, 941−950.
(27) Zhang, J. Y., Chen, W. L., and Zhang, C. C. (2009) hetR and patS, two genes necessary for heterocyst pattern formation, are widespread in filamentous nonheterocyst-forming cyanobacteria. *Microbiology 155*, 1418−1426.
(28) Risser, D. D., and Callahan, S. M. (2009) Genetic and cytological evidence that heterocyst patterning is regulated by inhibitor gradients that promote activator decay. *Proc. Natl. Acad. Sci. U.S.A. 106*, 19884−19888.
(29) Huang, X., Dong, Y., and Zhao, J. (2004) HetR homodimer is a DNA-binding protein required for heterocyst differentiation, and the DNA-binding activity is inhibited by PatS. *Proc. Natl. Acad. Sci. U.S.A. 101*, 4848−4853.
(30) Zhou, R., Wei, X., Jiang, N., Li, H., Dong, Y., Hsi, K. L., and Zhao, J. (1998) Evidence that HetR protein is an unusual serine-type protease. *Proc. Natl. Acad. Sci. U.S.A. 95*, 4959−4963.
(31) Zhou, R., Cao, Z., and Zhao, J. (1998) Characterization of HetR protein turnover in Anabaena sp. PCC 7120. *Arch. Microbiol. 169*, 417−423.
(32) Dong, Y, Huang, X, Wu, X. Y., and Zhao, J. (2000) Identification of the active site of HetR protease and its requirement for heterocyst differentiation in the cyanobacterium Anabaena sp. strain PCC 7120. *J. Bacteriol. 182*, 1575−9.
(33) Risser, D. D., and Callahan, S. M. (2007) Mutagenesis of hetR reveals amino acids necessary for HetR function in the heterocystous cyanobacterium Anabaena sp. strain PCC 7120. *J. Bacteriol. 189*, 2460−2467.
(34) Wu, X., Liu, D., Lee, M. H., and Golden, J. W. (2004) patS minigenes inhibit heterocyst development of Anabaena sp. strain PCC 7120. *J. Bacteriol. 186*, 6422−6429.
(35) Khudyakov, I. Y., and Golden, J. W. (2004) Different functions of HetR, a master regulator of heterocyst differentiation in Anabaena sp. PCC 7120, can be separated by mutation. *Proc. Natl. Acad. Sci. U.S.A. 101*, 16040−16045.
(36) Reeves, R., and Nissen, M. S. (1990) The A.T-DNA-binding domain of mammalian high mobility group I chromosomal proteins. A novel peptide motif for recognizing DNA structure. *J. Biol. Chem. 265*, 8573−8582.
(37) Banks, G. C., Mohr, B., and Reeves, R. (1999) The HMG-I(Y) A.T-hook peptide motif confers DNA-binding specificity to a structured chimeric protein. *J. Biol. Chem. 274*, 16536−16544.
(38) Goodwin, G. H., and Johns, E. W. (1973) Isolation and characterisation of two calf-thymus chromatin non-histone proteins with high contents of acidic and basic amino acids. *Eur. J. Biochem. 40*, 215−219.
(39) Goodwin, G. H., Sanders, C., and Johns, E. W. (1973) A new group of chromatin-associated proteins with a high content of acidic and basic amino acids. *Eur. J. Biochem. 38*, 14−19.
(40) Grosschedl, R., Giese, K., and Pagel, J. (1994) HMG Domain Proteins - Architectural Elements in the Assembly of Nucleoprotein Structures. *Trends Genet.*, 94−100.
(41) Reeves, R., Leonard, W. J., and Nissen, M. S. (2000) Binding of HMG-I(Y) imparts architectural specificity to a positioned nucleosome on the promoter of the human interleukin-2 receptor alpha gene. *Mol. Cell. Biol. 20*, 4666−4679.
(42) Huth, J. R., Bewley, C. A., Nissen, M. S., Evans, J. N., Reeves, R., Gronenborn, A. M., and Clore, G. M. (1997) The solution structure of an HMG-I(Y)-DNA complex defines a new architectural minor groove binding motif. *Nat. Struct. Biol. 4*, 657−665.
(43) Kim, Y., Joachimiak, G., Ye, Z., Binkowski, T. A., Zhang, R., Gornicki, P., Callahan, S. M., Hess, W. R., Haselkorn, R., and Joachimiak, A. (2011) Structure of transcription factor HetR required for heterocyst differentiation in cyanobacteria. *Proc. Natl. Acad. Sci. U.S.A. 108*, 10109−10114.
(44) Elhai, J., and Wolk, C. P. (1988) Conjugal transfer of DNA to cyanobacteria. *Methods Enzymol. 167*, 747−754.
(45) Limphong, P., Crowder, M. W., Bennett, B., and Makaroff, C. A. (2009) Arabidopsis thaliana GLX2−1 contains a dinuclear metal binding site, but is not a glyoxalase 2. *Biochem. J. 417*, 323−330.
(46) Schneider, D., Freed, J. (1989) Calculating slow motional magnetic resonance spectra: A user's guide, in *Biological Magnetic Resonance* (Berliner, L., Reuben, J., Eds.), pp 1−76, Plenum, New York, NY.
(47) Budil, D., Lee, S., Saxena, S., and Freed, J. (1996) Nonlinear-least-squares analysis of slow-motion EPR spectra in one and two dimensions using a modified Levenberg-Marquardt algorithm. *J. Magn. Reson., Ser. A*, 155−189.
(48) Hoofnagle, A. N., Stoner, J. W., Lee, T., Eaton, S. S., and Ahn, N. G. (2004) Phosphorylation-dependent changes in structure and dynamics in ERK2 detected by SDSL and EPR. *Biophys. J. 86*, 395−403.
(49) Zhang, Z., Fleissner, M. R., Tipikin, D. S., Liang, Z., Moscicki, J. K., Earle, K. A., Hubbell, W. L., and Freed, J. H. (2010) Multifrequency electron spin resonance study of the dynamics of spin labeled T4 lysozyme. *J. Phys. Chem. B 114*, 5503−5521.
(50) Nesmelov, Y. E., Agafonov, R. V., Burr, A. R., Weber, R. T., and Thomas, D. D. (2008) Structure and dynamics of the force-generating domain of myosin probed by multifrequency electron paramagnetic resonance. *Biophys. J. 95*, 247−256.
(51) Jeschke, G., Chechik, V., Ionita, P., Godt, A., Zimmermann, H., Banham, J., Timmel, C., Hilger, D., and Jung, H. (2006) DeerAnalysis2006—a comprehensive software package for analyzing pulsed ELDOR data. *Appl. Magn. Reson.*, 473−498.
(52) Chiang, Y. W., Borbat, P. P., and Freed, J. H. (2005) The determination of pair distance distributions by pulsed ESR using Tikhonov regularization. *J. Magn. Reson. 172*, 279−295.
(53) Phillips, J. C., Braun, R., Wang, W., Gumbart, J., Tajkhorshid, E., Villa, E., Chipot, C., Skeel, R. D., Kalé, L., and Schulten, K. (2005) Scalable molecular dynamics with NAMD. *J. Comput. Chem. 26*, 1781−1802.
(54) Humphrey, W., Dalke, A., and Schulten, K. (1996) VMD: visual molecular dynamics. *J. Mol. Graphics 14* (33−38), 27−38.
(55) Polyhach, Y., Bordignon, E., and Jeschke, G. (2011) Rotamer libraries of spin labelled cysteines for protein studies. *Phys. Chem. Chem. Phys. 13*, 2356−2366.
(56) Frías, J. E., Flores, E., and Herrero, A. (1997) Nitrate assimilation gene cluster from the heterocyst-forming cyanobacterium Anabaena sp. strain PCC 7120. *J. Bacteriol. 179*, 477−486.
(57) Borthakur, P. B., Orozco, C. C., Young-Robbins, S. S., Haselkorn, R., and Callahan, S. M. (2005) Inactivation of patS and hetN causes lethal levels of heterocyst differentiation in the

filamentous cyanobacterium Anabaena sp. PCC 7120. *Mol. Microbiol. 57*, 111−123.
(58) Klug, C. S., Eaton, S. S., Eaton, G. R., and Feix, J. B. (1998) Ligand-induced conformational change in the ferric enterobactin receptor FepA as studied by site-directed spin labeling and time-domain ESR. *Biochemistry 37*, 9016−9023.
(59) Buchaklian, A. H., and Klug, C. S. (2005) Characterization of the Walker A motif of MsbA using site-directed spin labeling electron paramagnetic resonance spectroscopy. *Biochemistry 44*, 5503−5509.
(60) Hanson, S. M., Francis, D. J., Vishnivetskiy, S. A., Kolobova, E. A., Hubbell, W. L., Klug, C. S., and Gurevich, V. V. (2006) Differential interaction of spin-labeled arrestin with inactive and active phosphorhodopsin. *Proc. Natl. Acad. Sci. U.S.A. 103*, 4900−4905.
(61) Fanucci, G. E., and Cafiso, D. S. (2006) Recent advances and applications of site-directed spin labeling. *Curr. Opin. Struct. Biol. 16*, 644−653.
(62) Klug, C. S., and Feix, J. B. (2008) Methods and applications of site-directed spin labeling EPR spectroscopy. *Methods Cell Biol. 84*, 617−658.
(63) Altenbach, C., Marti, T., Khorana, H. G., and Hubbell, W. L. (1990) Transmembrane protein structure: spin labeling of bacteriorhodopsin mutants. *Science 248*, 1088−1092.
(64) Mchaourab, H. S., Lietzow, M. A., Hideg, K., and Hubbell, W. L. (1996) Motion of spin-labeled side chains in T4 lysozyme. Correlation with protein structure and dynamics. *Biochemistry 35*, 7692−7704.
(65) Mchaourab, H. S., Kálai, T., Hideg, K., and Hubbell, W. L. (1999) Motion of spin-labeled side chains in T4 lysozyme: effect of side chain structure. *Biochemistry 38*, 2947−2955.
(66) Milov, A., Ponomarev, A., and Tsvetkov, Y. (1984) Electron electron double-resonance in electron-spin echo—model biradical systems and the sensitized photolysis of decalin. *Chem. Phys. Lett.*, 67−72.
(67) Milov, A., Salikhov, K., and Shirov, M. (1981) Application of ELDOR in electron-spin echo for paramagnetic center space distribution in solids. *Fiz Tverd Tela (Leningrad) 23*, 957−982.
(68) Borbat, P. P., Davis, J. H., Butcher, S. E., and Freed, J. H. (2004) Measurement of large distances in biomolecules using double-quantum filtered refocused electron spin-echoes. *J. Am. Chem. Soc. 126*, 7746−7747.
(69) Borbat, P., Freed, J. (2001) *Double Quantum ESR and Distance Measurements*, Kluwer, New York, NY.
(70) Higa, K. C., and Callahan, S. M. (2010) Ectopic expression of hetP can partially bypass the need for hetR in heterocyst differentiation by Anabaena sp. strain PCC 7120. *Mol. Microbiol. 77*, 562−574.
(71) Harrison, S. C. (1991) A structural taxonomy of DNA-binding domains. *Nature 353*, 715−719.
(72) Latchman, D. S. (1997) Transcription factors: an overview. *Int. J. Biochem. Cell Biol. 29*, 1305−1312.
(73) Huffman, J. L., and Brennan, R. G. (2002) Prokaryotic transcription regulators: more than just the helix-turn-helix motif. *Curr. Opin. Struct. Biol. 12*, 98−106.
(74) Feig, A. L. (2007) Applications of isothermal titration calorimetry in RNA biochemistry and biophysics. *Biopolymers 87*, 293−301.
(75) Streicher, W. W., Lopez, M. M., and Makhatadze, G. I. (2009) Annexin I and annexin II N-terminal peptides binding to S100 protein family members: specificity and thermodynamic characterization. *Biochemistry 48*, 2788−2798.
(76) Connelly, P. R., Aldape, R. A., Bruzzese, F. J., Chambers, S. P., Fitzgibbon, M. J., Fleming, M. A., Itoh, S., Livingston, D. J., Navia, M. A., and Thomson, J. A. (1994) Enthalpy of hydrogen bond formation in a protein-ligand binding reaction. *Proc. Natl. Acad. Sci. U.S.A. 91*, 1964−1968.
(77) Calderone, C. T., and Williams, D. H. (2001) An enthalpic component in cooperativity: the relationship between enthalpy, entropy, and noncovalent structure in weak associations. *J. Am. Chem. Soc. 123*, 6262−6267.
(78) Williams, D. H., Stephens, E., O'Brien, D. P., and Zhou, M. (2004) Understanding noncovalent interactions: ligand binding energy and catalytic efficiency from ligand-induced reductions in motion within receptors and enzymes. *Angew. Chem., Int. Ed. 43*, 6596−6616.
(79) Harishchandra, G., McCarrick, R. M., Budil, D. E., and Lorigan, G. A. (2009) Significantly improved sensitivity of Q-Band PELDOR/DEER experiments relative to X-Band is observed in measuring the intercoil distance of a leucine zipper motif peptide (GCN4-LZ). *Biochemistry 48*, 5782−5784.